

Interface of epitaxial SrTiO₃ on silicon characterized by transmission electron microscopy, electron energy loss spectroscopy, and electron holography

H. F. Tian, H. X. Yang, H. R. Zhang, Y. Li, H. B. Lu, and J. Q. Li*

Beijing National Laboratory for Condensed Matter Physics, Institute of Physics, Chinese Academy of Sciences, Beijing 100080, People's Republic of China

(Received 20 November 2005; published 23 February 2006)

The interfacial oxygen diffusion during film growth often results in the appearance of a thin SiO_x layer in SrTiO₃/Si films and related heterojunctions. High-resolution TEM investigations on the La_{0.9}Sr_{0.1}MnO₃/SrTiO₃/Si(LSMO/STO/Si) heterojunctions suggested that the thickness and microstructure of the SiO_x interfacial layer change visibly from one sample to another grown under slightly different conditions. Electron diffraction observations demonstrated the epitaxial relationships in the LSMO/STO/Si heterojunction as $[001]_{\text{LSMO}} \parallel [-110]_{\text{Si}}$, $[110]_{\text{LSMO}} \parallel [001]_{\text{Si}}$ and $[001]_{\text{STO}} \parallel [001]_{\text{Si}}$, $[010]_{\text{STO}} \parallel [-110]_{\text{Si}}$. The electron energy loss spectroscopy analyses on the LSMO/STO/Si interfacial region indicated that the Si ions are in intermediate oxidation states in the amorphous layer and the interfacial Ti bonding changes slightly. Electron holography measurements indicated that the energy barrier between the Si substrate and the LSMO film is about 0.95 ± 0.16 V, where notable negative charges accumulate in the amorphous SiO_x layer.

DOI: [10.1103/PhysRevB.73.075325](https://doi.org/10.1103/PhysRevB.73.075325)

PACS number(s): 68.37.Lp, 61.14.Nm, 79.20.Uv, 79.60.Jv

I. INTRODUCTION

Since the discovery of colossal magnetoresistance (CMR) in the perovskite manganese oxides, there has been enormous interest in these kinds of materials and related devices because of their unusual magnetic and electronic properties and possible potential applications, such as magnetic field sensors, hard disk read heads, magnetic tunnel junctions, and *p-n* junctions.¹⁻³ In order to combine the advantages of functional oxides with Si electronics, several insulating oxide films, e.g., SrTiO₃, BaTiO₃, and Bi_{3.25}La_{0.75}Ti₃O₁₂, were epitaxially deposited on a Si substrate.^{4,5} The main driving forces behind these efforts is the application of the current complementary metal-oxide-semiconductor technology on silicon. Recently, efforts^{6,7} have been made to grow manganese oxide films on certain buffered semiconducting substrates, Lü *et al.*⁸ have fabricated the La_{1-x}Sr_xMnO₃/SrTiO₃, La_{1-x}Sr_xMnO₃/SrTiO₃/Si, and La_{1-x}Sr_xMnO₃/Si heterojunctions and found the ultrafast photoelectric effects expanding the application prospect. The nature of the interface in the thin films, heterojunctions, and related devices plays a crucial role in their physical properties. Interface roughness and composition inhomogeneity across the interface can evidently affect the optical and electronic parameters.^{9,10} Hence, understanding of electronic structure, energy barriers, and charge diffusion in these newly developed heterojunctions and related semiconducting devices is one of the crucial issues in both academic research and technological applications. In addition to transmission electron microscopy (TEM) and electron energy loss spectroscopy (EELS), the rapidly developed electron holography has also been successfully applied in studies of interfaces,¹¹ and grain boundaries.¹² Electron holography measurements in combination with theoretical analysis can directly reveal the interface diffuseness, the electric potential, and field crossing of a semiconducting *p-n* junction.¹³ In this paper, we will report on the remarkable interfacial modifications arising from the oxygen diffu-

sion between the SrTiO₃ (STO) film and Si substrate in the related heterojunctions as observed by TEM, EELS, and electron holography.

II. EXPERIMENT

The La_{0.9}Sr_{0.1}MnO₃ (LSMO) films were fabricated by a computer-controlled laser molecular beam epitaxy. The Si substrates were first dipped into a ~5% HF solution for 20 ~ 30 s to remove the native silicon oxide on the surfaces and to form a hydrogen-terminated surface, and then were immediately transferred into the epitaxial chamber. The SrO and STO with a thickness of about 1 to 2 nm were deposited on the Si substrate as buffer layers at room temperature, then the LSMO film was subsequently deposited. Samples for TEM observations were prepared using the conventional method consisting of gluing, cutting, mechanical polishing, dimpling, and finally ion thinning using the FISCHIONE 1010. The specimen was milled from both sides using an acceleration voltage of 3.5 kV and an incident angle of 12°. Before insertion into the TEM for structural investigations, the specimen has been carefully cleaned in plasma cleaner to remove carbon contamination. A Tecnai-F20 (200 kV) FEG-TEM equipped with a Gatan image filter system was used to examine the microstructure and to acquire EELS in the interface regions of LSMO/STO/Si films. Electron microscopy and off-axis electron holography observations were carried out using a Philips CM200/FEG-TEM equipped with an electrostatic biprism. A Möllenstedt-Düker electrostatic biprism was used to interfere beams from different parts of the illuminated area. The holograms were acquired with a Gatan 794 multiscan charge coupled device camera and processed using the HOLOWORK package.

III. RESULTS AND DISCUSSION

We will first focus our attention on the interfacial alteration arising from oxygen diffusion between STO and Si.

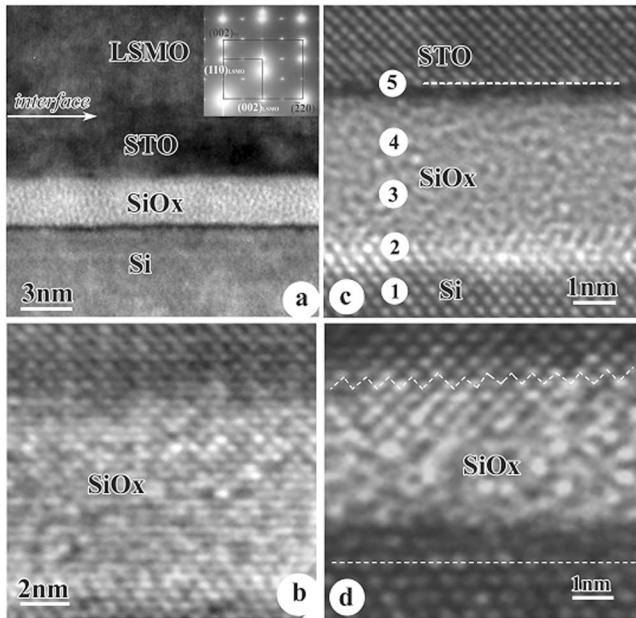


FIG. 1. (a) High-resolution TEM image showing the morphology and layered structure of the epitaxial LSMO/STO/Si film indicating the presence of an amorphous layer. The corresponding SAED pattern is shown in the inset. (b) TEM image showing the visible crystal lattice fringe along the c direction. (c) Layer-by-layer type of atomic ordering for the interface between the STO and SiO_x layer. (d) Zigzag type of atomic ordering for the interface between the STO and SiO_x layer.

Figure 1(a) is a bright-field TEM image displaying the cross-section morphology and the epitaxial growth relationships of the as-grown LSMO/STO/Si film along the $\langle 001 \rangle$ direction of silicon. The essential layered structural feature in the LSMO/STO/Si heterojunction, as well as an interfacial amorphous (bright band), are clearly recognizable in the TEM images. The thickness for the LSMO, STO, and the amorphous layers as measured from the cross-sectional TEM images are about 1200 nm, 4 nm, and 3 nm, respectively. Columnar structures originating from the interface to the LSMO film commonly appear on this kind of film, as reported in previous investigations. This typical microstructure property is fundamentally connected with the growth mechanism and the interfacial misfit strain. The inset of Fig. 1(a) shows that the selected-area electron diffraction (SAED) pattern from the interface region clearly exhibits the diffraction spots arising distinctively from the Si substrate, STO, and LSMO films. The weak but sharp spots at the systematic position $\{h h 2n+1\}$ position are caused by the known buckling structural distortion in the perovskite LSMO. The growth direction of the LSMO film in general follows the $\langle 110 \rangle$ direction and occasionally follows the $\langle 001 \rangle$ direction in certain regions. The orientation relationships between the LSMO film and the Si substrate can be briefly described as $[001]_{\text{LSMO}} \parallel [-110]_{\text{Si}}$, $[110]_{\text{LSMO}} \parallel [001]_{\text{Si}}$ as indicated in the inset of Fig. 1(a). The diffraction spots for STO are weak owing to its small thickness, and the SAED pattern from the STO/Si film clearly demonstrate the orientation relationships of $[001]_{\text{STO}} \parallel [001]_{\text{Si}}$, and $[010]_{\text{STO}} \parallel [-110]_{\text{Si}}$. The lattice mis-

match in this case is fairly small, its theoretical value being about 1.7% for STO ($a=3.905 \text{ \AA}$) and Si $d_{110}=3.84 \text{ \AA}$.

To get a thorough understanding of the microstructure properties of the interfacial amorphous layer, we have performed an extensive investigation on several typical samples. The experimental results indicate that interfacial oxygen diffusion could markedly damage interfacial atomic structure and yields a notable disordered (amorphous) layer between the STO layer and the Si substrate. This disordered layer was considered as a slice of the interfacial silica¹⁴ caused by oxygen diffusion from the film into the Si during film deposition. This process is generally accompanied by the atomic reorganization in the interfacial region. According to our systematic analysis, as well as the TEM images reported in previous literature,¹⁵ this disordered layer has a thickness of 0.7 to 4 nm, and the atomic structural features depend directly on the local oxygen concentration in SiO_x . Figure 1(b) shows a high-resolution TEM image demonstrating the presence of a partially ordered state (intermediated state) for the reaction layers. The crystal lattice fringes along the growth c direction are clearly visible, in sharp contrast with the totally destroyed atomic order within the a - b plane. These results probably suggest that the interfacial oxygen diffusion results in the silicon disordering first within the a - b plane and then layer by layer along the c -axis direction. Though the thickness of the amorphous layers or atomic disordering could change notably depending on deposition conditions, these TEM observations clearly demonstrate that the deposited STO and film grows perfectly along the c -axis direction. The Si (001) surface in all images has a well-defined atomic structure as indicated by the dashed lines, suggesting that the interface between STO and the amorphous layer can be either wavy or sharp as exhibited in Fig. 1(c) and Fig. 1(d), respectively. These facts suggest that the oxidation of the Si substrate generally occurs layer by layer along the Si $\langle 001 \rangle$ direction. The influence of the amorphous layer on the STO growth is certainly complex and accompanied by the atomic disordering of the Sr, Ti, and O sublattices, as demonstrated in the following EELS analysis.

In order to clearly view the alternation of chemical composition and the valence states of the major atoms at the interfacial region, we have performed a series of EELS measurements from the Si substrate, via the SiO_x amorphous layer, to the STO film. Figure 2(a) shows the EELS spectra in the low energy range obtained from the areas in Fig. 1(c) as numbered 1 to 5. In order to well identify the local electronic structure, these spectra were obtained under scanning transmission electron microscopy (STEM) mode with a probe size of 0.3 nm in diameter (the SiO_2 spectrum¹⁶ is cited for comparison). Energy resolution in these spectra is about 0.9 eV for the FWHM (full width at half maximum) of the zero-loss peak. The most striking feature is the progressive shift of the plasma peak at around 17.2 eV in Si to 24.6 eV in SiO_2 . This fact directly suggests that the amorphous layer is actually in the intermediate states of SiO_x with x ranging from 0 to 2, it is also noted that the peaks in spectra 2, 3, and 4 are quite broad; this phenomenon is considered a result of the different oxidation states in the detected area.

The EELS measurements of the near-edge structures for Si-L and Ti-L edges were performed using a probe size of

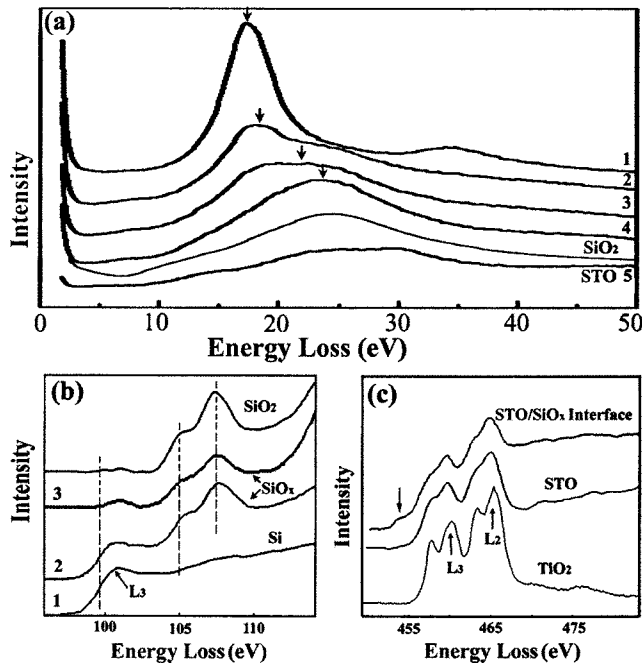


FIG. 2. (a) EELS spectra in the low energy range obtained from the areas in Fig. 1(c) as numbered 1 to 5, (b) Near-edge structure of Si- L_{3} from the Si substrate and SiO_x layer, the SiO₂ spectrum is cited for comparison. (c) Near-edge structure of Ti- $L_{2,3}$ from the STO layer and a small area at the STO/SiO_x interface, showing the presence of additional pre-edge structures. The Ti- $L_{2,3}$ peaks in TiO₂ is cited for illustrating the Ti⁴⁺ spectrum.

about 1.5 nm in diameter. It is noted that the EELS near-edge structures for Si- L and Ti- L edges show up evident alternation depending on the probe position. Figure 2(b) shows the EELS near-edge structures for Si- L_{3} from the areas indicated in Fig. 2(b), i.e., the Si substrate labeled 1 and two different areas within the SiO_x layer labeled 2 and 3. The SiO₂ spectrum cited from the EELS atlas is also shown for comparison. The remarkable L -edge shift from Si through SiO_x toward SiO₂, can be well understood in terms of state alternation of Si oxidation. The broadening of the L_{3} edges on SiO_x directly suggests the presence of multioxide states arising from the interfacial reaction accompanying the atomic disordering. Previously, the electronic structure for the Si-SiO₂ interface has been investigated by x-ray photoelectron spectroscopy¹⁷ and by an EELS equipped¹⁸ TEM. The spectral features revealed in near-edge structures can be fundamentally interpreted for the transitions from the $2p$ state to the conducting band; these critical transition energies are, respectively, 99.8 eV for bulk silicon and 106 eV and 108 eV for SiO₂ (Si⁴⁺). The spectra from interfacial areas show the presence of broadened peaks ranging from 102 eV to 104 eV, suggesting the existence of SiO and certain mixed states. Si atoms in a SiO (Si²⁺) crystal are coordinated by two oxygen and two Si atoms and could give rise to a transition of about 103 eV as indicated by the arrow in Fig. 2(b). Figure 2(c) shows the EELS near-edge structures of Ti- $L_{2,3}$ obtained respectively from the STO layer and a small area at the STO/SiO_x interface. The Ti- $L_{2,3}$ peaks in TiO₂ is cited for illustrating the typical Ti⁴⁺ spectrum. It is remarkable that

certain additional fine structures appear at pre-edge regions for the interfacial Ti ions. This result directly suggests that the local Ti-O bonding changes notably during interfacial oxygen diffusion.

In addition to the notable changes of the atomic structure and electronic structure on the interfacial region, the influence of interfacial oxygen diffusion on the charge density (electrons or holes) in the heterojunctions is another focal point of the present study. Electron holography measurements in principle can provide information on the distribution of electrostatic potential due to charge accumulation. When the electron beams pass through a local electric field, interaction between the incident electron wave and the electrostatic potential within the specimen induces a local differential phase shift in the exit electron wave function. If the sample is free from magnetic fields, the phase difference between the object wave and the reference wave is given by

$$\Delta\phi(x,y) = C_E \int V(x,y,z) dz, \quad (1)$$

where C_E is a constant [$C_E = 7.295 \times 10^{-3}$ rad/(V nm) for 200 keV electron], $V(x,y,z)$ is the electrostatic potential of the object including intrinsic and extrinsic fields. The integral is taken along a trajectory parallel to the beam direction.

In the interface region, the phase changes on the junction are directly connected with the potential barrier and charge distribution. Under experimental conditions with minimal dynamic diffraction effects, the phase shift of the object wave is given by

$$\Delta\phi(x,y) = C_E [V_0 t + V_{pn}(t - 2t_0)], \quad (2)$$

where t is the sample thickness, and t_0 is the thickness of the amorphous layer on each sample surface (mainly induced during the TEM sample preparation and can be partially removed in a plasma cleaner), V_0 is the mean inner potential (MIP) of the specimen. For high-energy electron beams, V_0 can be determined by the classical electrostatic potential of an atom in the solid. As the phase profile is obtained as a line scan across the junction in the present investigation, the phase shift and the interfacial potential can be written as

$$V_{pn} = \frac{\Delta\phi(x)}{C_E t(x)} - V_0. \quad (3)$$

For a sample with thickness described by $t(x)$ along the line-scan trace and ignoring the thickness of a dead layer, the magnitude of the potential V_{pn} can also be calculated from the charge distribution $\rho(x)$ using Poisson's equation

$$\frac{d^2}{dx^2} V_{pn}(x) = -\frac{\rho(x)}{\epsilon\epsilon_0}, \quad (4)$$

where ϵ is the relative permittivity and ϵ_0 is the permittivity of a vacuum. Solving the above equations yields two important parameters—the barrier height and the depletion region width.

Figure 3(a) shows an electron hologram from this junction, the interference fringe spacing is about 0.16 nm, which gives a spatial resolution of about 0.5 nm. The hologram is taken with the junction oriented parallel to the electron bi-

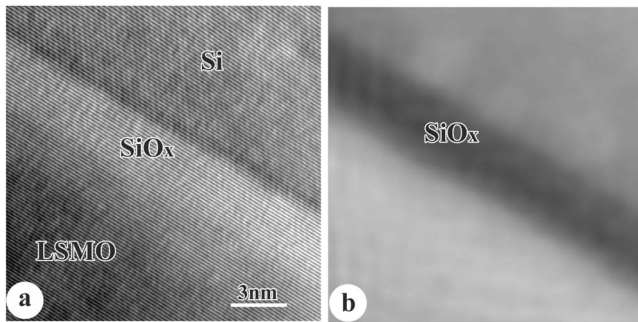


FIG. 3. (a) Hologram taken on the interface for LSMO/STO/Si film. (b) Reconstructed phase image from obtained hologram, demonstrating the presence of remarkable phase changes across the heterojunction.

prism wires, and the electron beam oriented perpendicular to the junction. Both the film and substrate are under weak diffraction conditions. Figure 3(b) is the reconstructed phase image from one set of holograms. The dark band of about 3 nm width at the center of the figure is the SiO_x layer, clearly showing the contrast alternations across interfaces in the heterojunction. The reconstructed amplitude image [not shown here] was used to derive the sample thickness profile following the method proposed by McCartney *et al.*¹⁹ The mean free path is estimated to be 90 nm for the Si and LSMO inelastic scattering. The local thickness for the distinctive layer in this junction can also be obtained using convergent

electron beam diffraction and EELS techniques.²⁰

Figure 4(a) shows the thickness profile (open triangle line) along the direction perpendicular to the junction, each data point is averaged laterally over 50 pixels to improve the signal statistics. The region of the Si substrate was set as the reference point to measure the relative thickness changes. It is found that the LSMO layer in this TEM cross-section sample is much thicker than the Si substrate, which is caused by the notable difference in ion milling rates between Si and LSMO materials in our TEM sample preparation. We can fit the thickness profile with a sigmoidal function (solid line) and get the average thickness difference of around 36 nm between Si and LSMO. Figure 4(b) shows the average phase profile from the reconstructed phase image (open square line). This measurement was performed at the same positions as the thickness profile. It is demonstrated that the phase decreases rapidly and reaches a minimum value at the center SiO_x layer, then the phase increases with a large slope and becomes positive in the STO and LSMO films. The phase difference is about 1.1 ± 0.2 rad on the junction as measured from Fig. 4(b).

It is known that a careful analysis of electron holography data requires a comprehensive consideration of other factors which influence the phase of the exit electron wave: (i) thickness variations, (ii) the MIP alternations across the junction, (iii) diffraction effects; and (iv) the presence of electrostatic fields within the specimen. The effects of fringing fields may be ignored because the width of the interfacial deletion layer is far less than the thickness of the sample.²¹ We can also

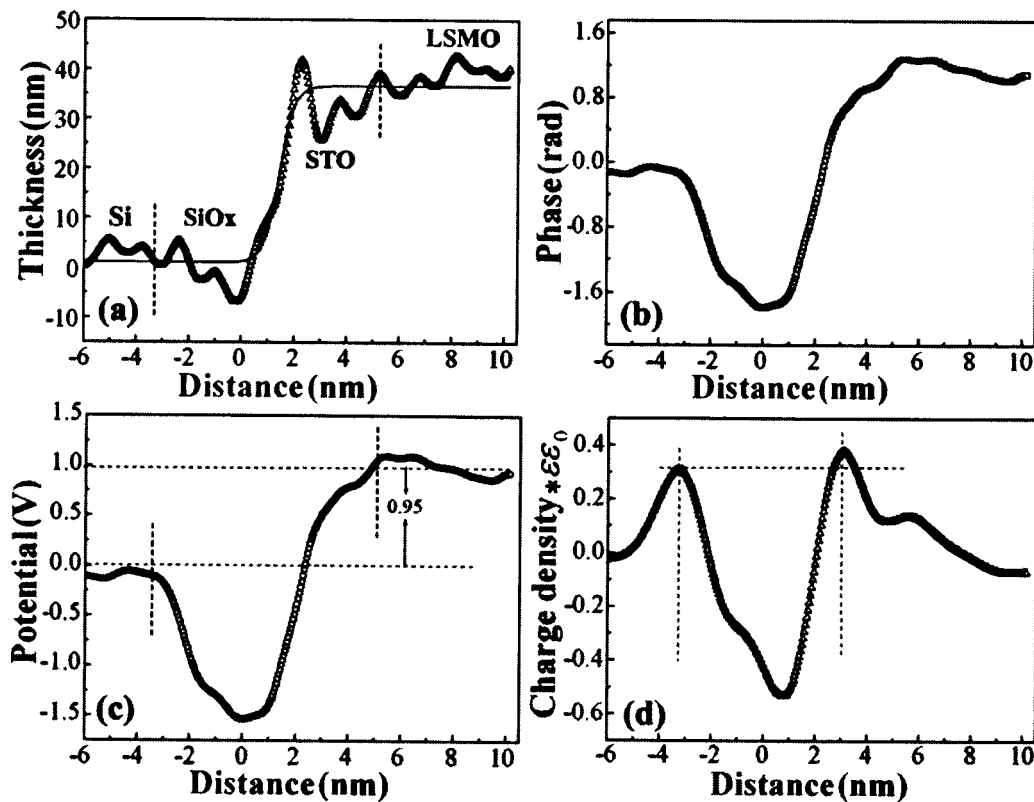


FIG. 4. (a) Thickness profile from a reconstructed amplitude image across the heterojunction. (b) Phase profile from the reconstructed phase image. (c) Potential profile across the junction after convolution of the thickness and subtracting the MIP offset from the phase profile. (d) Charge distributions from Poisson's equation.

eliminate the diffraction effects by tilting the sample off the zone axis. In the present investigation, we are interested in the electrostatic potential distribution across the heterojunction, therefore, the first two items are mainly considered in the following analysis.

Equation (3) states that the phase difference depends on the electrostatic potential distribution in the specimen. Normalizing to the thickness is needed to quantify the experimental results. Though the wedge shape is usually found in the specimens prepared using ion milling, in the present case, the thickness of the Si substrate and LSMO film, with evident ion-milling rate, can be considered separately in the close vicinity of the junction. Measurements of the substrate and the film are performed through recording another hologram, where the thickness is obtained from the reconstructed amplitude image. The averaged thicknesses as measured in the present experiment are 36 nm for Si and 72 nm for LSMO. These results are in good agreement with the data measured by low loss EELS spectra.

The MIP is a fundamental property of a solid and given by the zero-order Fourier component of the crystal potential. The values are typically between -5 and -30 V, depending on composition and structure. Our approach to determine the MIP is from the phase shift for the known thickness as discussed in the above context. From the measured slopes for both the phase and the thickness in this junction, an approximation of the MIP from several areas of the sample gave a value of 10.8 ± 1.8 V for Si and 7.6 ± 1.3 V for LSMO. The result for the Si substrate data is basically consistent with the theoretical value of 14.2 V using the nonbinding approximations.²²

Figure 4(c) shows the resultant potential profile across the junction after convolution of the thickness and subtracting the MIP offset from the phase profile, the barrier height between the Si substrate and the LSMO film is 0.95 ± 0.16 V as demonstrated by the broken line. The potential variations look similar with the phase profile, which drop to the minimum value at the center of the silicon oxide layer, and rise steeply on the interface region adjacent to the SiO_x/STO interface. The width of the layer is estimated to be around 4 nm. The depletion region width estimated from the potential

profile extends approximately 10 nm. The noise fluctuation of the potential profile is considered as arising from the fringing field. Figure 4(d) shows the corresponding charge distribution obtained from Poisson's equation. It is notable that there are two bumps at the interface positions indicating the positive charge accumulated in the Si/SiO_x region and the SiO_x/STO interface as indicated by the dotted line. The negative charges accumulate mainly in the center SiO_x layer resulting from the interfacial diffusion in the heterojunction. These facts directly demonstrate that the interfacial reaction, such as oxygen diffusion in the present case, can cause remarkable alternations in both atomic structures and charge distribution. A more detailed study for understanding the effect of interfacial structures on the fundamental properties of these heterojunctions is now in progress.

IV. CONCLUSIONS

In summary, we have performed an extensive investigation on the interfacial properties of the LSMO/STO/Si heterojunctions by means of TEM, EELS, and electron holography. It is found that the thickness and microstructure of the SiO_x interfacial layer change clearly from one sample to another, grown under slightly different conditions. Electron diffraction observations show the epitaxial relationships of the LSMO/STO/Si films and substrates as $[001]_{\text{LSMO}} \parallel [-110]_{\text{Si}}$, $[110]_{\text{LSMO}} \parallel [001]_{\text{Si}}$ and $[001]_{\text{STO}} \parallel [001]_{\text{Si}}$, $[010]_{\text{STO}} \parallel [-110]_{\text{Si}}$. EELS analyses on the STO/Si interface indicated that the Si ions are in intermediate oxidation states in the amorphous layer, and the interfacial Ti bonding changes slightly due to oxygen diffusion. Electron holography measurements indicated that the energy barrier between the Si substrate and the LSMO film is about 0.95 ± 0.16 V, and notable negative charges accumulate in the amorphous SiO_x layer.

ACKNOWLEDGMENTS

The authors thank F. L. Wang for her assistance in preparing samples, and N. Pemberton-Pigott for his help during manuscript preparation. The work reported here was supported by the National Natural Science Foundation of China.

*Correspondence and requests should be addressed to J. Q. Li.
Email address: ljq@aphy.iphy.ac.cn

¹C. Mitra, P. Raychaudhuri, K. Dorr, K. H. Müller, L. Schultz, P. M. Oppeneer, and S. Wirth, *Phys. Rev. Lett.* **90**, 017202 (2003).

²J. Z. Sun, D. W. Abraham, K. Poche, and S. S. P. Parkin, *Appl. Phys. Lett.* **73**, 1008 (1998).

³H. B. Lu, S. Y. Dai, Z. H. Chen, Y. L. Zhou, B. L. Cheng, K. J. Jin, L. F. Liu, and G. Z. Yang, *Appl. Phys. Lett.* **86**, 032502 (2005).

⁴H. N. Lee, D. Hesse, N. Zakharov, and U. Gösele, *Science* **296**, 2006 (2002).

⁵R. A. McKee, F. J. Walker, and M. F. Chisholm, *Phys. Rev. Lett.* **81**, 3014 (1998); *Science* **293**, 468 (2001).

⁶Z. Trajanovic, C. Kwon, M. C. Robson, K. C. Kim, M. Rajeswari,

R. Ramesh, T. Venkatesan, S. E. Lofland, S. M. Bhagat, and D. Fork, *Appl. Phys. Lett.* **69**, 1005 (1996).

⁷A. Tiwari, A. Chug, C. Jin, D. Kumar, and J. Narayan, *Solid State Commun.* **121**, 679 (2002).

⁸H. B. Lü, K. J. Jin, Y. H. Huang, M. He, K. Zhao, Y. L. Zhou, B. L. Cheng, Z. H. Chen, S. Y. Dai, and G. Z. Yang, *Chin. Phys. Lett.* **21**, 2308 (2004); *Appl. Phys. Lett.* **86**, 241915 (2005).

⁹E. Y. Tsymbal and D. G. Pettifor, *J. Magn. Magn. Mater.* **202**, 163 (1999).

¹⁰K. J. Jin, H. B. Lu, Q. L. Zhou, K. Zhao, B. L. Cheng, Z. H. Chen, Y. L. Zhou, and G. Z. Yang, *Phys. Rev. B* **71**, 184428 (2005).

¹¹M. Gajdardziska-Josifovska, *Interface Sci.* **2**, 425 (1995).

¹²V. Ravikumar, R. P. Rodrigues, and V. P. Dravid, *Phys. Rev. Lett.*

- 75, 4063 (1995); K. D. Johnson and V. P. Dravid, *Appl. Phys. Lett.* **74**, 621 (1999).
- ¹³W. D. Rau, P. Schwander, F. H. Baumann, W. Höppner, and A. Ourmazd, *Phys. Rev. Lett.* **82**, 2614 (1999).
- ¹⁴V. Shuttanandan, S. Thevuthasan, Y. Liang, E. M. Adams, Z. Yu, and R. Droopad, *Appl. Phys. Lett.* **80**, 1803 (2002).
- ¹⁵Z. Yu, J. Ramdani, J. A. Curless, J. M. Finder, C. D. Overgaard, R. Droopad, K. W. Eisenbeiser, J. A. Hallmark, and W. J. Ooms, *J. Vac. Sci. Technol. B* **18**, 1653 (2000).
- ¹⁶C. C. Ahn, O. L. Krivanek, R. P. Burgner, M. M. Disko, and P. R. Swann, *EELS Atlas*, (Gatan, Inc., Warrenton, PA, 1983).
- ¹⁷X. M. Hu, H. Li, Y. Liang, Y. Wei, Z. Yu, D. Marshall, Jr., J. Edwards, R. Droopad, X. Zhang, A. A. Demkov, and K. Moore, *Appl. Phys. Lett.* **82**, 203 (2003).
- ¹⁸P. E. Batson, *Nature (London)* **366**, 727 (1993).
- ¹⁹M. R. McCartney, M. A. Gribelyuk, J. Li, P. Ronsheim, J. S. McMurray, and D. J. Smith, *Appl. Phys. Lett.* **80**, 3213 (2002).
- ²⁰R. F. Egerton, *Electron Energy-Loss Spectroscopy in the Electron Microscope*, 2nd ed. (Plenum, New York, 1996).
- ²¹G. Pozzi, *J. Phys. D* **29**, 1807 (1996).
- ²²M. Gajdardziska-Josifovska, A. H. Carim, E. Völkl, L. F. Allard, and D. C. Joy, *Introduction to Electron Holography* (Kluwer/Plenum, New York, 1999).